Available online at www.sciencedirect.com
SCIENCE DIRECT®
Microporous and Mesoporous Materials 81 (2005) 175–183
MICROPOROUS AND MESOPOROUS MATERIALS
www.elsevier.com/locate/micromeso

Template-assisted syntheses of two novel porous zirconium methylphosphonates

Zongbin Wu [a], Zhongmin Liu [a,*], Peng Tian [a], Yanli He [a], Lei Xu [a], Yue Yang [a], Yangyang Zhang [a], Xinhe Bao [b], Xiumei Liu [b], Xianchun Liu [b]

[a] *Natural Gas Utilization and Applied Catalysis Laboratory, Dalian Institute of Chemical Physics, Chinese Academy of Sciences, P.O. Box 110, Dalian 116023, PR China*

[b] *State Key Laboratory of Catalysis, Dalian Institute of Chemical Physics, Chinese Academy of Sciences, P.O. Box 110, Dalian 116023, PR China*

Received 28 June 2004; received in revised form 23 August 2004; accepted 28 January 2005
Available online 8 March 2005

Abstract

Two porous zirconium methylphosphonates (designated as ZMPmi and ZMPme respectively) were synthesized by using dibutyl methylphosphonate (DBMP) as a template. Two efficient post-synthetic treatments were developed to remove the incorporated template without destroying the hybrid structures. The materials were characterized by SEM, EPMA, TG, DTA, FTIR, and NMR. Specific surface area and porosity were evaluated by BET, α_s-plots and DFT methods based on N_2 adsorption–desorption isotherms. The specific surface areas of ZMPmi and ZMPme are determined to be 279 and 403 $m^2\,g^{-1}$ and the maxima of pore size distributions are at 0.7 and 1.3 nm respectively.

Keywords: Porous zirconium methylphosphonate; Template-assisted synthesis; Dibutyl methylphosphonate

1. Introduction

Numerous inorganic porous materials, featuring microporous, mesoporous, macroporous or hierarchically micro/meso/macroporous architectures, have been synthesized over the years by employing organic molecules, mainly amines or ammonium salts, as templates [1–5]. In most cases, an interesting matching exists between the geometry of an organic template and its host. By fine-tuning the size, shape, charge and concentration of the employed templates as well as the synthetic conditions, various porous structures could be formed [6–10]. For inorganic porous materials, the incorporated organic templates can be removed easily by heat treatment or other methods [11–13]. After removal of the template, useful open-porous materials are obtained for many applications, including catalysis, separation, sensors, membranes, molecular recognitions, and so on. In a word, using templates for synthesizing inorganic porous materials leads to significant breakthroughs in the fields.

Compared with the conventional inorganic porous materials, organic–inorganic hybrid porous materials (abbreviated as OIHPMs) are fairly new. The framework of an OIHPM is built up from both organic and inorganic moieties, which are connected strongly by covalent bonds. OIHPMs have many novel properties and potential applications and are drawing more and more attentions [1–4,14–16]. Although the template-assisted methods exhibit the above-mentioned merits, they are rarely employed in the area of synthesizing of OIHPMs. The main reason is that it is very difficulty for an OIHPM to retain its chemical integrity and

* Corresponding author. Tel.: +86 411 84685510; fax: +86 411 84691570.
E-mail address: liuzm@dicp.ac.cn (Z. Liu).

1387-1811/$ - see front matter © 2005 Elsevier Inc. All rights reserved.
doi:10.1016/j.micromeso.2005.01.031

porous structure during the process of removing the incorporated templates. Up to now, a few of OIHPMs were synthesized by the template-assisted method and the incorporated template was removed mainly by solvent extraction or thermal decomposition [17,18]. The former method consumed a large amount of liquid solvent and the latter one found narrow suitability. In order to revive the template-assisted methods in the field of OIHPMs, it is highly desirable to seek novel templates and exploring new host-guest interactions.

Zirconium phosphonates are a kind of typical OIHPM with a long research history [19]. Most members in the family exhibit layered structures. Attempts to synthesize porous zirconium phosphonates have been mainly based upon organically pillared biphosphonates or structurally modified biphosphonates with small spacer moieties. Relatively, the latter method gives more chance to obtain microporosity or mesoporosity [19–21]. According to Clearfield et al., the stacking of unequally sized layers could yield the pores. Thus, uncontrolled stacking and randomly-sized layers are the intrinsic difficulties that prevent preparing highly ordered porous zirconium phosphonates. Recently, the discovery of five metal phosphonates provides an impetus in synthesizing novel porous phosphonates. They are β-$Cu^{II}(O_3PCH_3)$ [22], β-$Al_2(O_3PCH_3)_3 \cdot H_2O$ (named as AlMepO-β) [23], α-$Al_2(O_3PCH_3)_3 \cdot nH_2O$ (named as AlMepO-α, $n = 0$–1.5) [24], $Co_2(O_3PCH_2PO_3) \cdot H_2O$ [25], and $UO_2(O_3PC_6H_5) \cdot 0.7H_2O$ [26]. The first four crystals have inorganic framework and unidimensional channels with organic lining. The last one has similar unidimensional channels with phenyl groups arranged on the outer periphery of the isolated channels. The most remarkable feature of AlMepO-β, AlMepO-α and $Co_2(O_3PCH_2$–$PO_3) \cdot H_2O$ is that their hybrid frameworks remain intact up to 723 K. More recently, we synthesized an aluminium methylphosphonate foam (named as AMPF) by using dibutyl methylphosphonates (DBMP) as the template [27]. The assembly of as-synthesized aluminum methylphosphonate and DBMP (designated as AMP) could be prepared conveniently at room temperature. After AMP was treated at 673 K and 10 mmHg for 2 h to remove the template, AMPF was formed. There are macropores and mesopores in AMPF and the mesopores exist in the walls of the macropores. Methyl groups bonded to the framework keep intact up to 792 K under air. In order to extend the applications of the method and to research it deeply, in this paper, we aim to synthesis novel porous zirconium methylphosphonates templated by DBMP, develop new post-synthetic treatments to remove the incorporated template, and investigate the effects of post-synthetic treatments on the structures of the end-products.

The focus of this article, zirconium methylphosphonate, possesses the highest thermal stability and largest specific surface area among the reported zirconium phosphonates [19,28,29]. In 1982, Dines and Griffith investigated the surface texture and crystallinity of zirconium bis(methylphosphonate) in detail [30]. They found that the specific surface area has an inverse relationship with the crystallinity (determined by X-ray diffraction). In addition, the difference in porosity was not a key factor in surface area determinations. In 1997, Jaffrès et al. reported a new method for preparing zirconium phosphonate materials by hydrolysis of dialkylphosphonate ester in-situ [31]. All of the zirconium methylphosphonates reported up to now possessed layered structures. Here, by using DBMP as the template and employing different post-synthetic treatment methods, two novel porous zirconium methylphosphonates were prepared.

2. Experimental

2.1. Materials

The reagents for synthesis, zirconium nitrate ($Zr(NO_3)_4 \cdot 5H_2O$), acetonitrile (CH_3CN), and benzene (C_6H_6), were analytical pure. A mixture of DBMP/MPA (MPA, methylphosphonic acid) was prepared by the same process reported by us previously and designated as DMM [27]. Results of ^1H NMR, GC–MS and elemental analysis ensured that DMM possessed the same component ratio (MPA:DBMP = 1.3:1 in mole) as that used before.

2.2. Synthesis of ZMPmi and ZMPme

(ZMPmi, microporous zirconium methylphosphonate; ZMPme, micro/mesoporous zirconium methylphosphonate). Thirty gram of zirconium nitrate and 16 ml DMM were dispersed in 60 ml acetonitrile under stirring at room temperature. After 30 min, 150 ml benzene was added into the above mixture and stirred for 30 min. When 500 ml deionized water was poured into the mixture, a white precipitate was formed immediately. The precipitate massed and floated between the water and the organic mixture when stirring was stopped. The precipitate was centrifuged, washed with deionized water for three times, and dried at 343 K (1.5 mmHg). Then, the as-synthesized assembly of zirconium methylphosphonate and DBMP was produced and designated as ZMP. Elemental analysis of ZMP gave the following composition (wt%): C 13.2, H 4.6, P 7.5, and Zr 35.2 (yield 95%, based on Zr).

After ZMP was treated at 573 K and 2×10^{-2} Torr for 4 h to remove the template, ZMPmi was formed. Elemental analysis of ZMPmi gave the following composition (wt%): C 5.4, H 1.6, P 7.1, and Zr 55.1. The as-synthesized ZMPmi prefers sticking to the wall of the quartz treater; therefore, there is weight loss during

the transferring process. The Zr-based yield is 90% for ZMPmi.

Eight gram ZMP and 100 ml deionized water were added successively into a 200 ml polytetrafluoroethylene-lined steel autoclave. The mixture was hydrothermally treated at 433 K for 24 h. The product was centrifuged, washed with deionized water for three times, and dried at 343 K (1.5 mmHg), and then ZMPme was obtained. Elemental analysis of ZMPme gave the following composition (wt%): C 3.0, H 1.1, P 7.5, and Zr 58.3 (yield 91%, based on Zr).

2.3. Characterization

Scanning electron microscope (SEM) images were obtained with a JSM-5600.

Map analyses of P and Zr were carried out on an electron probe microanalysis analyzer (EPMA 1600, Shimadzu Corporation, Japan), operated under an accelerating voltage of 15.0 kV, a probe current of 3×10^{-8} A and a probe electron beam diameter of 1 μm. The powder samples were dusted onto conductive adhesive tapes for determination.

Thermogravimetric (TG) and differential thermal analysis (DTA) measurements of the samples were recorded on a Perkin Elmer Pyriss TGA and a Perkin Elmer DTA7 equipment separately, with a heating rate of 5 K/min from 323 K to 1073 K under air (20 ml/min). The "real time" TG–MS analysis of ZMP was carried out on a spectrometer Omnistar™ (Blazers Instruments). The sample was ionized by the electron impact method. First, a full scan from *m*/*z* 10 to 80 was performed to observe the key fragments, then a set of selected mass numbers (*m*/*z*) was chosen and scanned for every 50 ms. The heating rate was 5 K/min from 323 K to 973 K under an air flow of 20 ml/min. A needle valve was used to regulate the gas flow from TG to MS for maintaining the vacuum for the MS vacuum.

Nitrogen gas adsorption–desorption isotherms of ZMPmi and ZMPme were measured on a Micromeritics ASAP-2010 apparatus at 77 K. Prior to the measurements, the samples were outgassed at 523 K for 6 h. Specific surface areas of the materials under study were calculated using the BET method on the basis of the adsorption data in relative pressure range from 0.04 to 0.3. Both microporosity and mesoporosity were evaluated by high-resolution α_s-plot [32,33]. An octyldimethylsilyl (ODMS)-modified LiChrospher Si-1000 Silica (RO1) was used as reference adsorbent [34]. Pore size distributions (PSD) for the samples were calculated using the DFT plus software provided by Micromeritics Instrument Corporation.

FTIR spectra were measured on a Bruker EQUINOX 55 FTIR spectrometer with a resolution of 4 cm^{-1}. For ZMP, ZMPmi and ZMPme, potassium bromide (KBr) was used as a support and a pure KBr pellet was used to correct the background. In order to investigate the process of template removal in ZMP, an in-situ cell equipped with ZnSe windows (Spectra-Tech) was used for high temperature and low-pressure experiments. A pure sample was pelletized, put into the cell and heated at different temperature from 373 to 773 K in vacuum (2×10^{-2} Torr) for 30 min.

^{13}C CP/MAS NMR (MAS, magnetic angle spinning) and ^{31}P MAS NMR were recorded at room temperature on a Bruker DRX-400 Spectrometer with BBO MAS probe at a magnetic field of 9.4 T, with a resonance frequency of 128.4 MHz for ^{13}C and 161.9 MHz for ^{31}P. The spin rates of the samples were 4 and 6 KHz for ^{13}C and ^{31}P, respectively. The chemical shifts were referenced to a saturated aqueous solution of sodium 4, 4-dimethyl-4-silapentane sulfonate (DSS) for ^{13}C and 85% H_3PO_4 for ^{31}P.

GC–MS analysis was carried out on a HP6890 GC–MS. The gas chromatograph was fitted with a HP5 capillary column (30 m × 0.25 mm). Helium (0.7 ml/min) was used as the carrier gas. The oven was heated at 333 K for 2 min, then the temperature was raised from 333 K to 553 K at 10 K/min, and held at 553 K for 20 min. The assignment of the ion current chromatogram was referenced to the Nist98_1 library.

3. Results and discussion

3.1. Morphologies and elemental distributions

Fig. 1 displays the SEM images of ZMPmi and ZMPme. The two images resemble each other and show irregular particles that link together forming irregular macropores.

EPMA mapping analyses of P and Zr in ZMPmi and ZMPme, and the corresponding secondary electron micrographs, are shown in Fig. 2. Generally, the higher the analyzed elemental concentration in a sample, the brighter the color in the EPMA photograph. For the two samples under study, the variation of brightness and densities of P and Zr in a sample synchronizes perfectly, which confirms that the elemental distributions of ZMPmi and ZMPme are homogeneous.

3.2. Thermal stability of the hybrid structures

Thermal analyses were performed in order to characterize the thermal stabilities of the hybrid structures in air under normal pressure. The results are given in Fig. 3(a) and (b). The initial weight loss is before 369 K, accompanied with an endothermic DTA peak below 408 K, which can be attributed to the loss of adsorbed water. The initial weight loss for ZMP is 20.7%, whereas for ZMPmi and ZMPme, they only show weight losses of 4.2% and 1%, respectively. The weight

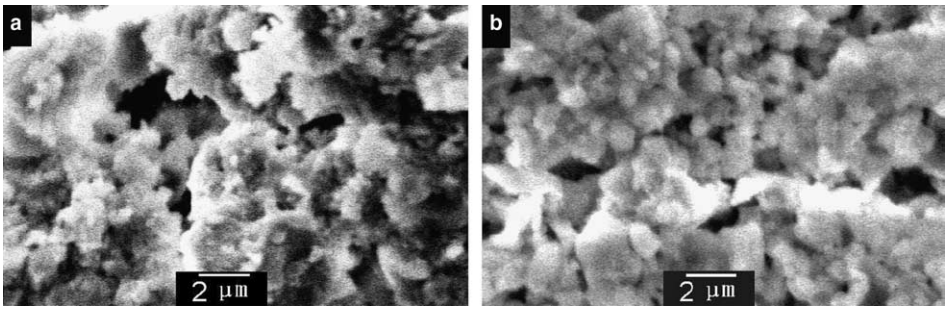

Fig. 1. SEM images of ZMPmi (a) and ZMPme (b).

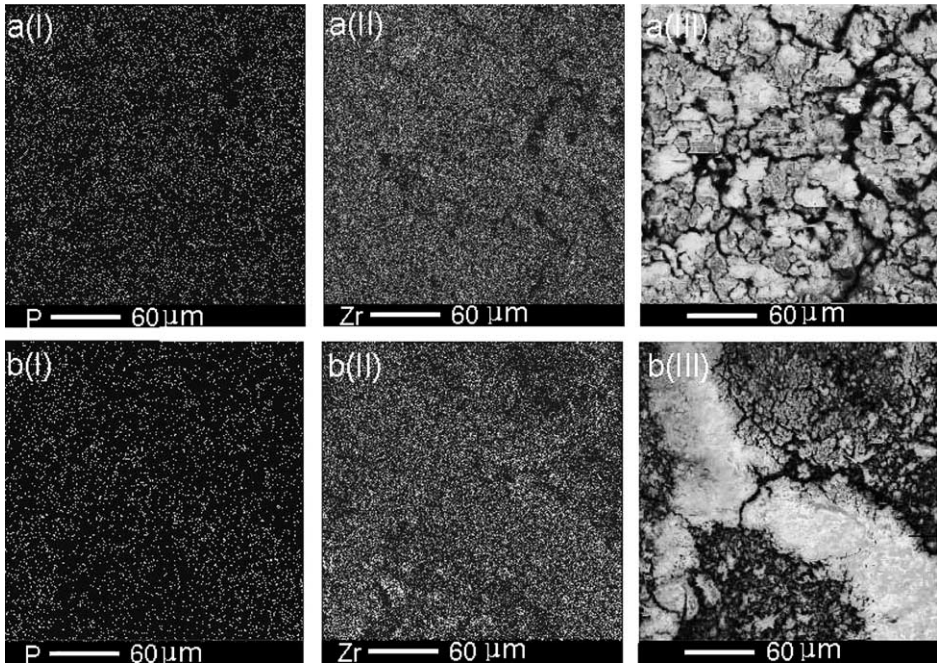

Fig. 2. EPMA mapping analyses of P (I) and Zr (II) in ZMPmi (a) and ZMPme (b) with corresponding secondary micrographs (III).

loss due to the removal of DBMP between 369 and 631 K is observed for ZMP (23.4%) and ZMPmi (2.8%). The process will be discussed in detail in the following paragraph with the help of "real time" TG–MS. For ZMPmi, the residual DBMP causes this weight loss. No weight loss occurs for ZMPme in this stage, which indicates that DBMP have been eliminated thoroughly by the hydrothermal treatment. The three samples exhibit a similar behavior in the TG curves between 730 and 852 K, because of the removal of the methyl groups in the samples. The weight losses are 2.2% (ZMP), 3.1% (ZMPmi), and 3.8% (ZMPme). This suggests that the hybrid structures of ZMPmi and ZMPme are stable up to 730 K in air.

Details of the processes involved in the removal of DBMP and methyl groups from ZMP were investigated by "real time" TG–MS. A full scan from *m*/*z* 10 to 80 was carried out first to determine the key fragments. Subsequently, a set of representative *m*/*z* of 12, 15, 14, 27, 28, 29, 32, 41, 42, 43, 44, 56, and 57 was chosen and measured by the MID method (multiple ion detection). The representative curves of *m*/*z* 15, 41, and 44 are shown in Fig. 3(c). The curves corresponding to hydrocarbon species (C_xH_y, $x \geqslant 2$; 14, 27, 28, 29, 32, 41, 42, 43, 56, and 57) are similar and illustrated by the curve of *m*/*z* 41 (Fig. 3c (I)). The curve has two peaks at 509 and 538 K, which implies that the process was more complicated than a simple decomposition and combustion. Perhaps, it involved different bound states of DBMP in ZMP. Further research should be done for its clear interpretation. The curves of *m*/*z* 44 and 12 assigned to CO_2 and carbenium ion respectively show the same profiles and are illustrated by the curve of *m*/*z* 44 (Fig. 3c (II)). It has three peaks centering at 506, 562, and 774 K. The curve of *m*/*z* 15 assigned to methyl group exhibits three peaks at 509, 538, and 777 K (Fig. 3c (III)). The appearance of peaks at 774 K in Fig. 3c (II) (assigned to CO_2) and 777 K in Fig. 3c (III) (assigned

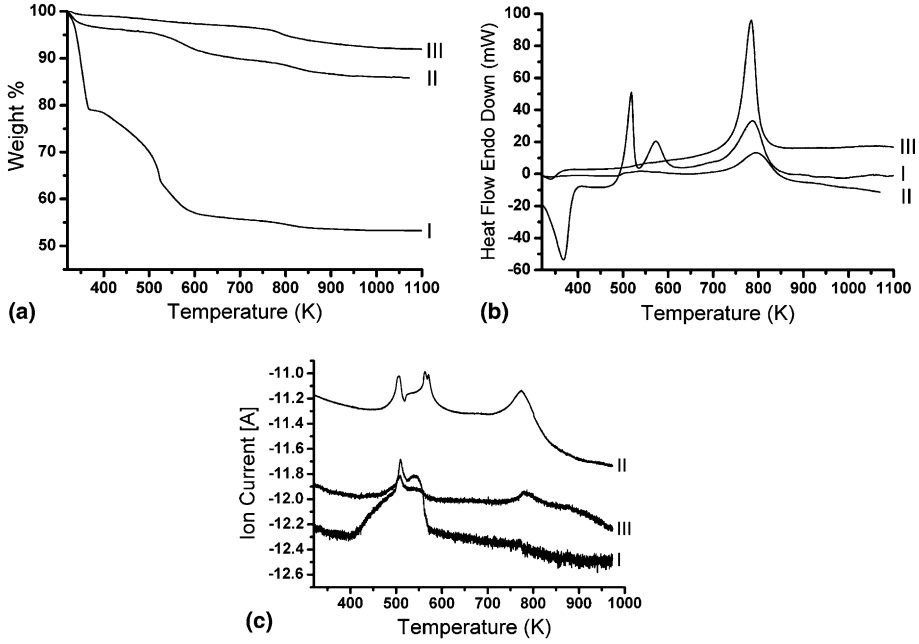

Fig. 3. TG (a) DTA (b) curves of ZMP (I), ZMPmi (II) and ZMPme (III); MS curves (c) of ZMP (ion current curves for *m*/*z* 15 (I), 41 (II) and 44 (III)).

to methyl group) indicate the good thermal stabilities of the hybrid structures. From the MS results, it is clear that the removal of DBMP and methyl groups in ZMP included two reactions, namely, the decomposition and the combustion reactions.

3.3. Specific surface area and porosity of ZMPmi and ZMPme

Fig. 4 shows the nitrogen adsorption–desorption isotherms of ZMPmi and ZMPme. The nitrogen adsorption isotherm of ZMPmi is of Type I, which indicates that ZMPmi is a microporous material. For ZMPme, the shape of the adsorption isotherm can be considered as a mixture of typical Type I and Type II isotherms. The initial part of the adsorption isotherm of ZMPme shows a steep uprising step which represents microporous filling, and the slope of the plateau at highly relative pressure is due to multilayer adsorption on mesoporous, macroporous or external surface. The shape of the hysteresis loop of ZMPme is of typical H4 type [35]. Therefore, there are micro- and mesopores in ZMPme.

A comparing method, the α_s-plot, is used to distinguish microporosity from mesoporosity for a sample with a complex porosity structure. It is carried out by comparing the adsorption isotherm of a sample under study with that of a reference adsorbent [36,37]. Fig. 5

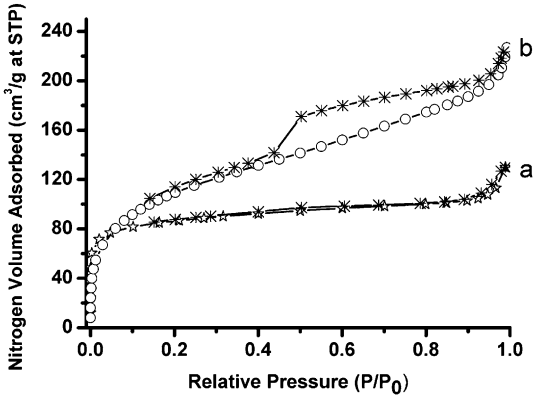

Fig. 4. Nitrogen adsorption–desorption isotherms of ZMPmi (a) and ZMPme (b) (☆ and ○: adsorption, ✳: desorption).

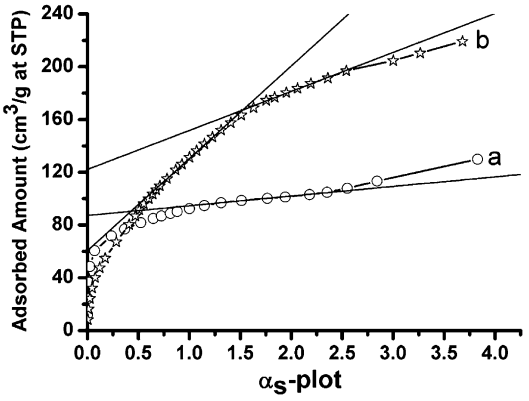

Fig. 5. α_s-plots of ZMPmi (a) and ZMPme (b) with RO1 (ODMS LiChrospher Si-1000 Silica) used as a reference.

shows the α_s-plots of ZMPmi and ZMPme, constructed by using reported data of RO1. For the two samples, a upward swing at $0 < \alpha_s < 0.75$ proves clearly that there are enhanced adsorbent–adsorbate interactions due to the micropores in ZMPmi and ZMPme. Because there are no clear steps in the two α_s-plots at about $\alpha_s = 0.4$, the total specific surface areas could not be calculated precisely by the subtracting pore effect method [36]. For ZMPmi, the α_s-plot has a linear region at $1.0 < \alpha_s < 2.25$, from which microporous volume (V_{mi}) and extra specific surface area (S_{ext}) can be calculated from the intercept and slope of the linear region. In contrast, there are two linear regions in the α_s-plot of ZMPme at $0.8 < \alpha_s < 1.5$ and $1.75 < \alpha_s < 2.5$, respectively. V_{mi} and the sum of S_{ext} and mesoporous specific surface area (S_{me}) are calculated from the intercept and slope of the first linear region; Meanwhile, the sum of V_{mi} and the mesoporous volume (V_{me}) and S_{ext} are calculated from the intercept and slope of the second linear region. All of the above mentioned porous parameters are listed in Table 1.

The curves of PSD calculated from the DFT method are shown in Fig. 6. The PSD of ZMPmi gives a narrow peak with the maximum at 0.7 nm, while the PSD of ZMPme shows a broad peak between 1.2 and 3.6 nm with the maximum at 1.3 nm. Concerning the Type I isotherm of nitrogen adsorption of ZMPmi, the other three peaks are tentatively assigned to artifact effects introduced by modeling assumptions. In summary, the shapes of N_2 adsorption–desorption isotherms, the calculated results of the α_s-plots and DFT methods support that there are micropores in ZMPmi and micro/mesopores in ZMPme.

3.4. Efficient post-synthetic treatments to remove the incorporated template

DBMP, used as the template in synthesizing ZMP, could be removed by thermal and hydrothermal treatments. Based on the different post-synthetic treatments, two porous zirconium methylphosphonates, ZMPmi and ZMPme, could be obtained. FTIR, NMR and GC–MS were used to investigate the structures of the materials and the process of template removal.

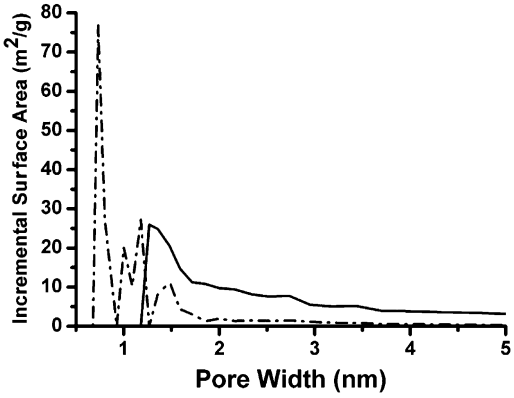

Fig. 6. Incremental pore size distributions for ZMPmi (dash dot) and ZMPme (solid) calculated by application of the DFT method to N_2 adsorption isotherms at 77 K.

3.4.1. As-synthesized ZMP

The infrared spectrum of ZMP is shown in Fig. 7(a). The band assigned to PO_2 vibration appears at 1035 cm^{-1} and the bands assigned to Zr–O vibration appear at 783, 718, and 512 cm^{-1} [38,39]. The peak at 1314 cm^{-1} is assigned to P–CH_3 bond. Bands corresponding to symmetrical and asymmetrical C–H stretching of DBMP appear at 2962, 2935, 1466, and 1384 cm^{-1}. The band at 1281 cm^{-1} is assigned to $\nu_{P=O}$ and the bands at 916, 807, 769, and 445 cm^{-1} are attributed to P–O bonds in DBMP. Comparing with free DBMP, the $\nu_{P=O}$ band in ZMP shifts towards higher wavenumber [40]. The phenomenon indicates that the bound DBMP is located in an electron-negative environment. There is an unassigned band at 1550 cm^{-1} that appears in all spectra, which probably is a combination band or overtone from the strong bands observed at low wavenumbers. In all spectra, there is no evidence for the presence of bands belonging to acetonitrile or benzene, which suggests that no solvent is incorporated in the samples. Moreover, no meaningful information could be deduced from the bands at about 3421 and 1629 cm^{-1} that normally arise from the stretching and bending vibrations of adsorbed water, respectively, because no special protection has been taken to avoid the interference of water in the KBr and the atmosphere during the process of pelletizing and measurements.

Table 1
Porosity parameters calculated by BET, α_s-plot and DFT methods

Sample	S_{BET}[a] ($m^2\ g^{-1}$)	S_{mi}[b,c] ($m^2\ g^{-1}$)	S_{me}[b] ($m^2\ g^{-1}$)	S_{ext}[b] ($m^2\ g^{-1}$)	V_{tot}[b,d] ($cm^3\ g^{-1}$)	V_{mi}[b] ($cm^3\ g^{-1}$)	W_{DFT}[e] (nm)
ZMPmi	279	258	–	21	–	0.13	0.7
ZMPme	403	199	118	86	0.16	0.08	1.3

[a] Specific microporous surface area calculated by BET method.
[b] Calculated by α_s-plot method.
[c] S_{mi}: microporous specific surface area; $S_{mi} = S_{BET} - S_{me} - S_{ext}$.
[d] V_{tot}: the total volume of mesoporous volume and microporous volume.
[e] the maximum of PSD calculated by application of the DFT method to N_2 adsorption isotherms.

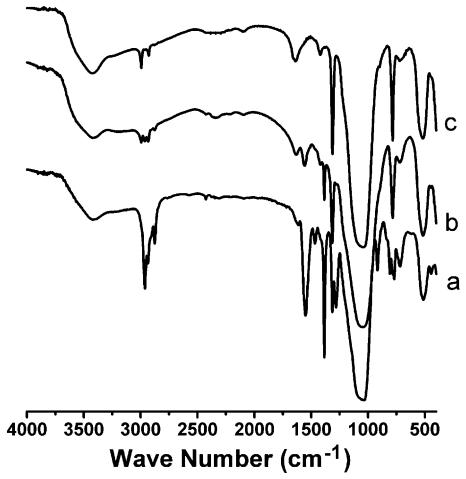

Fig. 7. FTIR spectra of ZMP (a), ZMPmi (b) and ZMPme (c).

Fig. 8(a) shows the ^{13}C CP/MAS NMR spectrum of ZMP. There are three well-resolved peaks at 66, 33, and 19 ppm, which are assigned to $O\underline{C}H_2$, $\underline{C}H_2$, and $\underline{C}H_2CH_3$ in DBMP (labeled by underline), respectively. The last broad peak contains other carbon species in DBMP ($\underline{C}H_3$ and $P\underline{C}H_3$) and MAP ($P\underline{C}H_3$).

The ^{31}P MAS NMR spectrum of ZMP is presented in Fig. 9(a). The relative molar ratio of the ^{31}P MAS NMR peaks after deconvolution is I:II = 1.3:1. In view of the molar ratio of MPA to DBMP in DMM (1.3:1), I and II could be assigned to MPA and DBMP, respectively. The agreement of MPA/DBMP molar ratio between DMM and the as-synthesized ZMP implies that MPA and DBMP assemble together in DMM under the reaction condition, and take part in the reaction as a whole.

3.4.2. ZMPmi obtained by thermal treatment of ZMP under vacuum

During the template removal from ZMP to form ZMPmi, the evaporation products were collected by

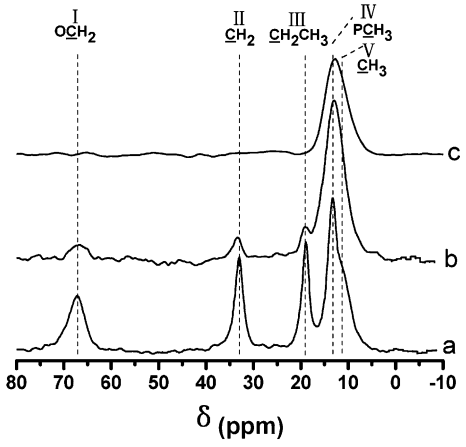

Fig. 8. ^{13}C CP/MAS NMR spectra of ZMP (a), ZMPmi (b) and ZMPme (c).

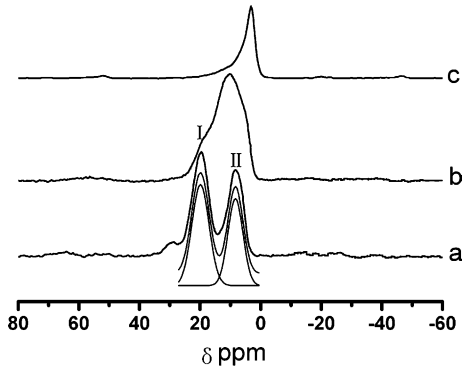

Fig. 9. ^{31}P MAS NMR spectra of ZMP (a), ZMPmi (b) and ZMPme (c) with the deconvoluted ^{31}P MAS NMR spectrum of ZMP.

condensation at 273 K and extracted with 60 ml water/carbon tetrachloride (CCl_4) (volume ratio of H_2O to CCl_4 equal to 1:1) for three times. The organic phase so obtained was analyzed by GC–MS. The evaporation products were only DBMP, which means that DBMP was removed from ZMP in molecular form.

Fig. 7(b) shows the FTIR spectrum of ZMPmi. The bands assigned to PO_2 vibration, Zr–O vibrations and P–CH_3 bond remain the same as those in the FTIR spectrum of ZMP. Bands assigned to the groups in DBMP present very weakly, which is due to the small remains of DBMP. In-situ FTIR spectra of ZMP were performed to study the process of DBMP removal during the thermal treatment under vacuum (see supplementary information). The representative bands of symmetrical and asymmetrical C–H stretching and P=O due to DBMP become weaker and weaker following the rising of temperature progressively. These bands vanish completely at 673 K, indicating that DBMP has been removed thoroughly. The changes are similar as that in AMP [27]. It is interesting to note that the methyl group in the hybrid structure keeps intact up to 773 K under the characterizing condition, which indicates the good thermal stability of the hybrid structure.

In the ^{13}C CP/MAS NMR spectrum shown in Fig. 8(b), the peaks assigned to DBMP become very weak and the most intense peak at 13 ppm is attributed to $P\underline{C}H_3$. A broad peak with the maximum at 10 ppm is observed in the ^{31}P MAS NMR spectrum (Fig. 9(b)) and the peak includes the sign assigned to the remains of DBMP. The results harmonize with that of FTIR.

3.4.3. ZMPme obtained by hydrothermal treatment of ZMP

After ZMP was treated by the hydrothermal method, the supernatant liquid in the autoclave was collected and extracted with 30 ml carbon tetrachloride for three times. The obtained organic phase was analyzed by GC–MS. Only *n*-butyl alcohol was observed. This implies that

DBMP was removed from ZMP through hydrolysis and the reaction could be deduced as follows:

$$(CH_3CH_2CH_2CH_2O)_2P(CH_3)O + 2H_2O \xrightarrow[\text{hydrothermal treatment}]{433\ K,\ 24\ h} (HO)_2P(CH_3)O + 2CH_3CH_2CH_2CH_2OH$$

Moreover, based on the elemental analysis, the molar ratios of P to Zr in ZMPmi and ZMPme are equal to 0.38. The fact rules out the possibility that MPA produced by the hydrolysis keeps in ZMPme.

The infrared spectrum of ZMPme is shown in Fig. 7(c). No bands assigned to DBMP are found. The rest bands keep the same as those in the spectra of ZMP and ZMPme.

There is only one peak at 12 ppm shown in ^{13}C CP/MAS NMR spectrum for ZMPme and assigned to $P\underline{C}H_3$ (Fig. 8(c)). In ^{31}P MAS NMR spectrum, a sharp and symmetrical peak at 3 ppm indicates a homogeneous environment of phosphorus in ZMPme (Fig. 9(c)).

Overall, compared with ZMP, the chemical shifts of phosphorus in ZMPmi and ZMPme move upfield clearly. According to Massiot et al. [41] and Zhang et al. [42], the phenomenon implies a bond-making process between phosphonate and zirconium during the removal of DBMP. That is, a restructuring occurs along with the post-synthetic treatments of ZMP, especially in the hydrolysis treatment.

Additionally, following the same hydrothermal treatment by which ZMPme was prepared, AlMepO-β crystals could be obtained by using AMP as the precursor. The products are pure and large enough to be studied by X-ray single crystal diffraction. The process had good repeatability and did not need any additives that were necessary to prepare the large AlMepO-β crystals [43]. Once more, two different porous hybrid materials, namely AMPF and AlMepO-β, could be obtained by using different post-synthetic treatments on AMP.

4. Conclusion

Two porous zirconium methylphosphonates, ZMPmi and ZMPme, were prepared by using DBMP as the template. DBMP could be removed from as-synthesized assembly of ZMP by evaporation in vacuum or by hydrothermal treatment, so that the intact hybrid porous structures with different specific surface areas and pore size distributions were obtained. EPMA mapping analyses of P and Zr in ZMPmi and ZMPme confirm the homogeneous distributions of the compositions. Thermal analyses indicate that the hybrid structures of the two porous materials are stable up to 730 K in air. The effectiveness of the two post-synthetic treatments on removal of template was verified by the results of FTIR and NMR. It is inferred from the NMR spectra that a bond-making process between phosphonate and zirconium occurs during the DBMP removal from ZMP.

Acknowledgement

The authors would like to acknowledge the support of the Knowledge Innovation Program of the Chinese Academy of Science (Grant: DICPK2000B3).

Supplementary data

Supplementary data associated with this article can be found, in the online version, at doi:10.1016/j.micromeso.2005.01.031.

References

[1] S. Andreas, Adv. Mater. 15 (2003) 763.
[2] S.C. Colin, A.C. Paul, Chem. Rev. 103 (2003) 663.
[3] J.de.A.A.S.-I. Galo, S. Clément, L. Bénédicte, P. Joël, Chem. Rev. 102 (2002) 4093.
[4] E. De.V. Dirk, D. Mieke, F.S. Bert, A.J. Pierre, Chem. Rev. 102 (2002) 3615.
[5] J.L. Blin, A. Léonard, Zh.Y. Yuan, L. Gigot, A. Vantomme, A.K. Cheetham, B.L. Su, Angew. Chem. Int. Ed. 42 (2003) 2872.
[6] H.P. Lin, Ch.Y. Mou, Acc. Chem. Res. 35 (2002) 927.
[7] H. Gies, B. Marler, Zeolites 12 (1992) 42.
[8] B.M. Lok, T.R. Cannan, C.A. Messina, Zeolites 3 (1983) 282.
[9] U. Ciesla, F. Schüth, Micropor. Mesopor. Mater. 27 (1999) 131.
[10] K.J.C.V. Bommel, A. Friggeri, S. Shinkai, Angew. Chem. Int. Ed. 42 (2003) 980.
[11] B.Zh Tian, X.Y. Liu, Ch.Zh Yu, F. Gao, Q. Luo, S.H. Xie, B. Tu, D.Y. Zhao, Chem. Commun. (2002) 1186.
[12] S. Kawi, M.W. Lai, Chem. Commun. (1998) 1407.
[13] T.J.K. Matthew, D. Renaud, L.L. Philip, Chem. Commun. (1998) 2203.
[14] W.J. Christopher, Science 30 (2003) 439.
[15] A.P. Wight, M.E. Davis, Chem. Rev. 102 (2002) 3589.
[16] L.J. Stuart, Chem. Soc. Rev. 32 (2003) 276 (and references therein).
[17] C.V. Nguyen, K.R. Carter, C.J. Hawker, J.L. Hedrick, R.L. Jaffe, R.D. Miller, J.F. Remenar, H.W. Rhee, P.M. Rice, M.F. Toney, M. Trollsås, D.Y. Yoon, Chem. Mater. 11 (1999) 3080.
[18] J.L. Hedrik, T. Magbitang, E.F. Connor, T. Glauser, W. Volksen, C.J. Hawker, V.Y. Lee, D.M. Robert, Chem. Eur. J. 8 (2002) 3309.
[19] A. Clearfield, Prog. Inorg. Chem. 47 (1998) 371 (and references therein).
[20] A. Clearfield, Chem. Mater. 10 (1998) 2801.
[21] G.B. Hix, A. Turner, B.M. Kariuki, M. Tremayne, E.J.J. MacLean, Mater. Chem. 12 (2002) 3220.
[22] J.L. Bideau, C. Payen, P. Palvadeau, B. Bujoli, Inorg. Chem. 33 (1994) 4885.
[23] K. Maeda, J. Akimoto, Y. Kiyozumi, F. Mizukami, Chem. Commun. 10 (1995) 1033.
[24] K. Maeda, J. Akimoto, Y. Kiyozumi, F. Mizukami, Angew. Chem. Int. Ed. 34 (1995) 1199.
[25] D.L. Lohse, S.C. Sevoy, Angew. Chem. Int. Ed. 36 (1997) 1619.
[26] D.M. Poojary, D. Grohol, A. Clearfield, Angew. Chem. Int. Ed. 34 (1995) 1508.

[27] Z.B. Wu, Zh.M. Liu, P. Tian, Y.L. He, L. Xu, X.M. Liu, X.H. Bao, X.Ch Liu, Micropor. Mesopor. Mater. 62 (2003) 61.
[28] K. Segawa, A. Sugiyama, Y. Kurusu, Stud. Surf. Sci. Catal. 60 (1991) 73.
[29] M.B. Dines, P.M. Digiacomo, Inorg. Chem. 20 (1981) 92.
[30] M.B. Dines, P.C. Griffith, Inorg. Chem. 86 (1982) 571.
[31] P.A. Jaffrès, V. Caignaer, D. Villemin, Chem. Commun. (1999) 1997.
[32] S.J. Gregg, K.S.W. Sing, Adsorption, Surface Area and Porosity, second ed., Academic Press, London, 1982.
[33] K. Kaneko, C. Ishii, H. Kanoh, Y. Hanzawa, N. Setoyama, T. Suzuki, Adv. Colloid Interface Sci. 76–77 (1998) 295.
[34] M. Kruk, V. Antochshuk, M. Jaroniec, J. Phys. Chem. B 103 (1999) 10670.
[35] F. Rouquerol, J. Rouquerol, K. Sing, Adsorption by Powders and Porous Solids, Academic Press, UK, 1999.
[36] N. Setoyama, T. Suzuki, K. Kaneko, Carbon 36 (1998) 1459.
[37] K.S.W. Sing, Adv. Colloid Interface Sci. 76–77 (1998) 3.
[38] G.B. Hix, K.D.M.J. Harris, Mater. Chem. 8 (1998) 579.
[39] W.T.A. Harrison, L.L. Dussack, A.J. Jacobson, Inorg. Chem. 35 (1996) 1461.
[40] L.L. Burger, J. Phys. Chem. B 62 (1958) 590.
[41] D. Massiot, S. Drumel, P. Janvier, M.B. Doeuff, B. Bujoli, Chem. Mater. 9 (1997) 6.
[42] B.L. Zhang, D.M. Poojary, A. Clearfield, Inorg. Chem. 37 (1998) 249.
[43] K. Maeda, J. Akimoto, Y. Kiyozumi, F. Mizukami, Stud. Surf. Sci. Catal. 105 (1997) 197.